Structural and biochemical characterization of VIM-26 show that Leu224 has implications for the substrate specificity of VIM metallo-β-lactamases

Hanna-Kirsti S. Leiros[1,*], Kine Susann Waade Edvardsen [1,a], Gro Elin Kjæreng Bjerga [1,b] and Ørjan Samuelsen[2]

[1] The Norwegian Structural Biology Centre (NorStruct), Department of Chemistry, UiT The Arctic University of Norway, N-9037 Tromsø, Norway

[2] Norwegian National Advisory Unit on Detection of Antimicrobial Resistance, Department of Microbiology and Infection Control, University Hospital of North Norway, N-9038 Tromsø, Norway.

[a] Current address: Department of Clinical Science, Section for Endocrinology, University of Bergen, N-5020 Bergen, Norway

[b] Current address: Uni Research AS, Centre for Applied Biotechnology, High Technology Centre, Thormøhlensgt. 55, N-5008 Bergen, Norway

* Corresponding author:

Hanna-Kirsti S. Leiros, E-mail: hanna-kirsti.leiros@uit.no, Phone +47 77 64 57 06

Running title: Structural and biochemical characterization of VIM-26

Abstract

Antimicrobial resistance has during the last decades become a global public health problem. Metallo-β-lactamases (MBLs) which are broad-spectrum β-lactamases that inactivate virtually all β-lactams including carbapenems, are contributing to this health problem. In this study a novel MBL variant, termed VIM-26, identified in a *Klebsiella pneumoniae* isolate was studied. VIM-26 belongs to the VIM-family of MBLs and is a His224Leu variant of the well-characterized VIM-1 variant. In this study, we report the kinetic parameters, minimum inhibitory concentrations (MICs) and crystal structures of a recombinant VIM-26 protein, and compare them to previously published data on VIM-1, VIM-2 and VIM-7. The kinetic parameters and MIC determinations show that VIM-26, like VIM-7 has higher penicillinase activity, but lower cephalosporinase activity than VIM-1 and VIM-2. The four determined VIM-26 crystal structures revealed mono- and di-zinc forms, where the Zn1 ion has distorted tetrahedral coordination geometry with an additional water molecule (W2) at a distance of 2.6 to 3.7 Å, which could be important during catalysis. The R2 drug-binding site in VIM-26 is more open compared to VIM-2 and VIM-7, and neutrally charged due to Leu224 but also because of Ser228. Thus, the VIM-26 drug-binding properties are different than in the VIM-2 (Tyr224/Arg228) and VIM-7 (His224/Arg228) structures, indicating a role of these residues in the substrate specificity.

Keywords: Antibiotic resistance, Metallo-β-lactamase, *Klebsiella pneumoniae*, drug binding site, minimum inhibitory concentrations.

Abbreviations: AMP, ampicillin; PIP, piperacillin; PTc, piperacillin-tazobactam; CAZ, ceftazidime; CTX, cefotaxime; CXM, cefuroxime; FOX, cefoxitin; FEP, cefepime: ATM, aztreonam; MEM, meropenem; IPM, imipenem; ETP, ertapenem; ESBL, extended-spectrum β-lactamase; MBL, metallo-β-lactamase; MIC, minimum inhibitory concentration; VIM, Verona integron-encoded metallo-β-lactamase; BBL, class B β-lactamase; PEG, Polyethylene glycol; PEG MME, polyethylene glycol monomethyl ethers.

Introduction

Antimicrobial resistance is not a new problem, but the increasing prevalence of antimicrobial resistance and multidrug-resistant bacteria has resulted in a growing public health problem [1]. In Gram-negative bacteria, the emergence and dissemination of acquired carbapenemases such as metallo-β-lactamases (MBLs) are of particular concern [2, 3]. MBLs hydrolyzes and inactivates all β-lactams including carbapenems with the exception of monobactams. The genes encoding MBLs are frequently located in mobile genetic structures facilitating dissemination and spread among Gram-negative bacteria [3]. Further, bacterial isolates harboring MBLs are often co-resistant to other antimicrobial agents such as aminoglycosides, thus limiting treatment options [3, 4].

The Verona integron-encoded metallo-β-lactamase (VIM) family currently includes >40 different VIM genes (http://www.lahey.org/Studies/) divided in the VIM-1, VIM-2 and VIM-7 subgroups [5]. VIM-26 was first reported in a clinical *Klebsiella pneumoniae* isolate from 2006 [6]. The isolate was found to be resistant to all β-lactams as well as aminoglycosides and ciprofloxacin and only susceptible to tigecycline and colistin [6]. VIM-26 differs from the well characterized VIM-1 by only one amino acid residue, a histidine to leucine substitution in position 224, and belongs to the VIM-1 subgroup. The amino acid sequence identity between VIM-26 and VIM-2 is 91%. Residue 224 is part of the loop including residues 223 to 240 named the L3 loop [7], L10 loop [8] or L2 loop [9, 10], and will herein be denoted the L3 loop. Mutagenesis studies of VIM-13 mutating Leu224 and Arg228 to His and Ser, respectively, as found in VIM-1, resulted in increased catalytic efficiency and elevated MIC values more similar to VIM-1, indicating the importance of the L3 loop [7]. In another study on VIM-23, which has just one amino acid difference compared to VIM-2, namely a serine at position 228 instead of an arginine as in VIM-2, a significant effect on MIC values in the same genetic background was observed with cephalosporins and ertapenem [11]. For other β-lactams the effect was similar between VIM-23 and VIM-2.

Residue 224 in the L3 loop, is a conserved lysine in many B1 family MBLs and found be critical for binding the carboxyl group on the C-3/C-4 atom of the substrate [2, 8, 12]. In the VIM family of enzymes residue 224 is found to be either a histidine such as in VIM-1, VIM-4, VIM-7 and VIM-31, a tyrosine such as in VIM-2 or a leucine such as in VIM-5, VIM-13, VIM-26 and VIM-28. We previously proposed, based on analysis of the crystal structure and docking experiments, that the His224 in VIM-7 was a residue determinant partly responsible for the poor affinity to positively charged cephalosporins [9, 13]. This was explained by the presence of a more positively charged R2 binding pocket repelling a positively charged substrate. In addition there are two stabilizing hydrogen bonds

in VIM-2 involving Tyr224 [9]. We later confirmed this through structural and kinetic studies of a His224Tyr mutation of VIM-7 where we could show that the mutant was more active against positively charged cephalosporins compared to the wild type VIM-7 [14]. In a VIM-2 thiol based inhibitor complex it was found that both Arg228 and Asn233 are important for inhibitor binding and recognition [15]. The L3 loop of VIM-4 and VIM-7 include His224 and Arg228 in both enzymes [9, 16], where His224 has a similar conformation in both enzymes. Arg228, however, points towards Zn2 in VIM-4, but has a more open conformation in VIM-7. Residue 228 is Ser in VIM-26 and VIM-1, but Arg in VIM-2, VIM-4, VIM-7 and VIM-31. All these finding underline the importance of residue 224 for the enzymatic activity and substrate specificity for this family of MBLs. Another loop important for the substrate specificity is the L1 loop (residues 60-66) situated opposite to the L3 loop, for example as shown for GIM-1 [10].

To characterize VIM-26 and explore the influence of the residue composition of the L3 loop on activity, we made a recombinant version the enzyme and subsequently performed enzyme kinetics studies, microbiological testing and determined four three-dimensional structures based on crystallization of recombinant VIM-26.

Results and discussion

The VIM-family of MBLs is along with the New Delhi Metallo-β-lactamase (NDM) family the most prevalent and widespread MBLs globally [3, 17]. Inhibition of serine-β-lactamases has previously been used successfully to extend the life-time of β-lactam antibiotics [18]. Despite promising scientific results [19], there is currently no clinically available inhibitor for MBLs [20]. Consequently, studies into the biochemical and structural characteristics of MBLs are important for future inhibitor design. In this study we have investigated the characteristics of VIM-26, a member of the VIM-MBL-family [6], in order to better understand the role of residue position 224 and particularly the L3 loop in substrate specificity.

Enzymatic characterization and MIC determinations

The steady state kinetic constants and MIC determinations for VIM-26 and the comparator enzymes (VIM-1, VIM-2 and VIM-7) are shown in Table 1 and Table 2, respectively. The kinetic experiments showed that recombinant VIM-26 hydrolyzes penicillins more efficiently than cephalosporins and carbapenems (Table 1; Figure 1). Among the penicillins tested we found that VIM-26 hydrolyzed benzylpenicillin more efficiently than ampicillin (Table 1). For the cephalosporins, VIM-26 was more efficient against cefuroxime compared to cefepime, ceftazidime and cefoxitin, mainly due to higher

affinity (lower K_M) but also higher turnover (higher k_{cat}) for the former. The relative carbapenemase activity of VIM-26 was similar between imipenem and meropenem, but slightly lower towards ertapenem, mainly due to lower affinity. The kinetic properties of VIM-26 were generally also observed in the MIC determinations with only marginal increases in the MIC to cefoxitin and ertapenem (Table 2).

Compared to the other VIM-variants, the overall trend was that VIM-26 and periplasmic purified VIM-7 [14] were more efficient penicillinases than VIM-1 [21] and VIM-2 [22] (Table 1). In contrast both VIM-1 (all cephalosporins) and to a certain degree VIM-2 (ceftazidime and cefoxitin) were more efficient cephalosporinases than VIM-26 and VIM-7. This was also in general reflected in the MIC values for most substrates (Table 2) except for some discrepancies (e.g. VIM-2 and ceftazidime). Kinetic analysis of VIM-5 [23] and VIM-13 [7] which along with VIM-26 also possesses Leu224 showed lower cephalosporinase activity compared to VIM-1 and VIM-2. This suggests that Leu224 could be involved in the lower cephalosporinase activity of VIM-26 as observed for other VIM-variants with Leu224. The catalytic efficiencies against the different carbapenems were found to be slightly lower for VIM-26 compared to VIM-1, VIM-2 and VIM-7. Generally, this could be attributed to lower binding affinities for these substrates since the turnover (k_{cat}) for VIM-26 against carbapenems were in many cases higher than for VIM-1, VIM-2 and VIM-7. It should be noted that the comparison of the kinetic properties of VIM-26 to other different VIM-variants were done using previously determined data from different laboratories. This could obviously influence the results. However, previous experience with VIM-2 revealed no major discrepancies with previously published values when tested under different experimental conditions (Samuelsen et al., 2008 [13]). Although the different VIM-genes were cloned into the same vector and *E. coli* background, the MIC values for some substrates did not correlate with the kinetic data. This could be due to several factors such as differences in enzyme expression, but could also indicate that *in vitro* determined properties do not always correlate to the *in vivo* setting.

The VIM-26 crystal structures

In order to gain further insight into the structure activity relationship of VIM-26, and to shed light on the role of Leu224 in the L3 loop, the crystal structure of the recombinant VIM-26 was solved (Figure 2).

From both cryo protected and inhibitor soaked crystals, we obtained in total four VIM-26 structures. The structures included one structure binding only one (Zn1) zinc ion (termed VIM-26-Mono), one

native structure (termed VIM-26) containing both the Zn1 (tri-histidine site) and Zn2 (Cys-His-Asp site) ions, one structure with an extra water molecule as the Zn1 ligand (termed VIM-26-W) and one structure with a PEG in the active site (termed VIM-26-PEG)(Figure 3). All structures are resolved to high resolution (1.55-1.70 Å), low R-factors (15.3-15.6%) and R-free values (18.2-20.0%) and satisfactory geometry (Table 3 and 4). The overall structure of VIM-26 showed, as expected, the characteristic αβ/βα fold of MBLs, with the active site situated at the edge of the ββ sandwich flanked by two catalytically important loops on each side consisting of residue 60-66 (denoted L1) and 223-240 (denoted L3) (Figure 2a).

The four VIM-26 structures had an RMDS value of 0.11-0.44 Å among each other for CA-atoms only, where VIM-26-Mono was the most diverse. Differences were found in the zinc binding sites of Zn1 and Zn2 (Table 5). Cys221 was oxidized into cysteinesulfonic residue in all VIM-26 structures (termed Osc221, Figure 3). Oxidation of Cys221 has also been observed in other subclass B1 MBLs (GIM-1, BcII, SPM-1)[10, 24, 25], indicating that this cysteine is an oxidative sensitive residue. The oxidation is likely explained by lack of reducing agents during crystallization since addition of the reducing agent (e.g. TCEP and β-mercaptoethanol) resolved this issue for both the VIM-2 and VIM-7 crystal structures [9, 26]. Still radiation damage [27, 28] of Cys221 at the highly intense BL14.1 beamline at Bessy-II cannot be ruled out.

The VIM-26-PEG structure was obtained after a soak with the inhibitor D-captopril but the extra electron density in the active site was interpreted as a PEG molecule and not the inhibitor. The PEG molecule is protruding into the R1 binding site where Trp87 is found in two conformations, but the overall structure is similar to the three other VIM-26 structures.

Zinc binding in the metallo-β-lactamase VIM-26

The Zn1 site in the four VIM-26 structures has either four (VIM-26, VIM-26-PEG) or five ligands (VIM-26-Mono, VIM-26-W) since an extra water molecule (W2) is bridging Zn1 and Asn233 ND2 in the two latter (Figure 3). The hydrogen bond from W2 to Asn233 ND2 (3.46 Å VIM-26-Mono; 3.09 Å in VIM-26-W) could be important for catalysis and/or substrate binding (Figure 3a, c). A similar water is found in the oxidised VIM-7 (PDB ID: 2Y8B)[9]. The role of residue 233 has been discussed as part of the substrate binding [29-32]. This residue is found to be asparagine in the majority of the B1 MBLs [31] including VIM-26, but is a tyrosine in other MBLs, for example in GIM-1 [10]. The fifth Zn1 ligand was found in both mono (VIM-26-Mono) and the di-zinc (VIM-26-W) forms, reflecting flexibility in the enzyme. The geometry of all Zn1 sites was tetrahedral (Table 5B) therefore the fifth Zn1 ligand could

resemble a carbonyl oxygen of an incoming substrate [9, 33]. A fifth Zn1 ligand is infrequently reported, but could be important here since it interacts with the partly conserved Asn233 residue in the L3 loop [31], the extra W2 water is adjacent the inhibitor bound to VIM-2 (PDB ID: 2YZ3; [15]), it interacts with the hydrolytic hydroxyl ion in-between two zinc ions and since water molecules are used in the hydrolyses of substrates and thus must be replaced during catalysis.

The Zn2 ion was missing in the VIM-26-Mono structure as judged from the observed electron density, thus indicating a lower zinc affinity for the Zn2 binding site compared to the Zn1 site. For the three other VIM-26 structures the geometry and interatomic distances of the Zn2 ion are a distorted octahedron with the Zn2 ion in the center, His263 NE2 and W1/hydroxyl ion at the axial positions, and Asp120 OD2, Ocs221 OD2 and two water molecules (W3, W4) at the four equatorial positions. The metal-to-metal distances are between 3.60 Å (VIM-26, VIM-26-W) to 3.86 Å (VIM-26-PEG; Table 5). The oxidised Cys221 has probably caused the reduced Zn2 occupancy (0.5 in VIM-26, 0.5 in VIM-26-W; 0.3 in VIM-26-PEG). Overall, the four presented structures shed light on the structural variation, flexible architecture and different coordination geometry of the metal centers in VIM-26. Despite the overall good quality electron density maps in the determined VIM-26 structures, we cannot completely rule out that the oxidised Cys221 disturbs its local environment.

The L1 loop

The main chain conformations of the L1 loop in the four VIM-26 structures were similar, but in VIM-26-Mono, the Gln59, Tyr67, His263, Trp87 and Asp119 residues were slightly shifted compared to the other structures. In the VIM-26-PEG structure, Trp87 was found in two different conformations. In the VIM-26-Mono structure Trp87 was slightly shifted and made a polar interaction with Asp119 OD2 (Figure 2c), whereas the Gln59 side chain was involved in a hydrogen bound to both Ala86 O (2.89 Å from NE2) and to Asn91 ND2 (3.11 Å from OE1). In the three other VIM-26 structures Gln59 NE2 was hydrogen bound to Trp87 O and the Gln59 side chain was water exposed. Tyr67 in the L1 loop of VIM-26-Mono was clearly rotated towards Trp87, although the OH-atoms were not defined in the observed electron density maps. Residue 87 is a tryptophan in all VIM crystal structures, found in one main rotamer conformation (VIM-2, VIM-4, VIM-7 [9, 15, 16, 26] and VIM-31 (PDB ID 4FSB, 4FR7)), except in oxidised VIM-31 (PDB ID: 4FSB). For VIM-26 it is also one preferable Trp87 conformation, and the one in VIM-26-Mono (Figure 2c) is less frequent and influenced by the adjacent residues. The movements of residues Gln59, Tyr67, His263, Trp87 and Asp119 in VIM-26-Mono could be also linked to the missing Zn2 ion, since the crystal packing, unit cell and space group were similar for all four structures.

Implication of Leu224 in the L3 loop

VIM-26 differs from VIM-1 by a single residue, namely histidine 224 which has been substituted with a leucine [6]. This residue is part of the L3 loop involved in the R2 substrate binding site, and plays an important role in catalysis [2, 7, 14]. All the VIM-26 structures showed an open binding site for the R2 part of the substrates (Figure 4a). We found that the electrostatic surface around the active site of VIM-26 showed a more neutral R2 site compared to VIM-2 and VIM-7 (Figure 4a, b, c), and also compared to VIM-4 (data not shown). According to our analysis of the structure, the substitution of histidine to leucine at position 224 is mainly responsible for the neutral R2 site in VIM-26, but Ser228 also contributes to generate a larger pocket. In both VIM-2 and VIM-7, residue 228 is arginine contributing to a narrower pocket. In two VIM-2 crystal structures, one apo-structure and one inhibitor bound (PDB ID: 1KO3 and 2YZ3, respectively) as well as in a VIM-7 structure (PDB ID: 2Y87), Arg228 are found in very different conformations [9, 15]. The mutation of His224 in VIM-7 into Tyr, to resemble the sequence of VIM-2, increased the thermal stability and enzyme activity of the mutant [14]. Furthermore, the enzymatic activity increased compared to wild type particularly towards the positively charged cephalosporins cefepime and ceftazidime [14], again underlining the importance of residue 224. Ser228 and Leu224 in VIM-26 make a very different binding site compared to Arg228 and Tyr/His224 in the other VIM structures (Figure 4a-c). The neutral residues in VIM-26 are also different from other B1 MBLs that have a conserved positively charged Lys224 in the R2 binding site [2, 8, 12], or Arg228 as in VIM-2 and VIM-7 structures [9, 15, 26]. This might explain the high K_M (lower affinity) found for VIM-26 compared to VIM-1, VIM-2 and VIM-7 for the cephalosporins and carbapenem substrates that all fill the R2 site upon biding.

Docking of the poorly catalyzed substrate ceftazidime (Figure 1) into VIM-26 showed more space in the R2 site with no hydrophobic nor polar interactions from the substrate to the VIM-26 enzyme. This could possibly reflect the low binding affinity found in our kinetics analysis (Table 1). The docking result does not, however, explain why the cephalosporins with positively charged or polar R2 groups are poorly catalyzed by VIM-26 with its neutral pocket for R2 binding. Phe61 and Asn233 in VIM-26 generate a “lid” over the metal binding site in all four VIM-26 structures. This is very different from what has been reported in VIM-2 (also with Phe61 and Asn233) and VIM-7 (with Leu61 and Asn233)(Figure 4a,b,c) where the entrance to metals in the active site is more accessible. Although this cannot be observed in our four VIM-26 crystal structures, we hypothesize that Phe61 and Asn233 can dissociate, and thereby open up the entry to the reactive metal center.

Conclusion

The enzymatic characterization and MIC determinations showed that VIM-26, like VIM-7 is characterized with being a more efficient penicillinase than VIM-1 and VIM-2, but with lower cephalosporinase activity. The only difference between VIM-1 and VIM-26 is the presence of Leu224 in VIM-26 instead of His224 in VIM-1, indicating the importance of this residue in the specificity of VIM-enzymes. Analysis of the determined VIM-26 crystal structures show that the L3 loop in VIM-26 which includes Leu224 and Ser228 make the R2 drug binding site both open and neutral. Such a neutral R2 binding site is different from many other B1 MBLs that has a conserved lysine at position 224 [2, 8, 12] reported to be important for binding the carboxyl group on the C-3/C-4 atom of the substrate. In VIM-2, VIM-4 and VIM-7, Arg228 can serve to make a similar substrate protein interaction as found in a VIM-2 inhibitor complex structure [15]. In contrast, VIM-26 cannot offer a similar positively charged residue for the substrate binding which might contribute to the specificity of VIM-26, and possibly explain why the penicillinase activity of VIM-26 is not affected by the presence of Leu224, but the cephalosporinase activity is reduced. Further, in our VIM-26-PEG structure the PEG molecule is found in the R1 drug binding site, surrounded by Phe61 in the L1 loop, Trp87, His118 and Asn233 in the L3 loop emphasizing a role of both the L1 and the L3 loops when binding to the enzyme.

The presented VIM-26 structures and characterization of VIM-26 have given further insights into the relationship between sequence, structure, and activity of VIM and subclass B1 MBLs, important for the future inhibitor design process.

MATERIALS AND METHODS

Cloning of *bla*$_{\text{VIM-26}}$ from *Klebsiella pneumonia* isolate U-60687

The *bla*$_{\text{VIM-26}}$ gene from a clinical *Klebsiella pneumoniae* isolate U-60687 [6], was amplified using the following primers VIM-26-NdeI: 5'-GGAATTC**CATATG**TTAAAAGTTATTAGTTTATTGG-3' and VIM-26-BamHI: 5'-CGC**GGATCC**CTACTCGGCGACTGAGCGATTTTTGTG-3' (*Nde*I and *Bam*HI restriction sites are indicated as bold and underscored bases). The PCR product was purified from the agarose gel using the QIAquick Gel extraction kit (Qiagen), digested with *Nde*I (NEB) and *Bam*HI (NEB), and ligated into the pET-26b expression vector (Novagen), generating the plasmid pET26b:VIM-26.

Expression and purification of VIM-26

VIM-26 was expressed and purified from the periplasm as previously described relying on the native leader sequence for transport [9, 13, 34]. In short, the pET26b:VIM-26 was transformed into *E. coli*

BL21(DE3) (Novagen). Transformed bacteria were grown in Terrific Broth supplemented with 50 mg/L kanamycin (Sigma) at 37°C. Expression was induced at mid log phase by addition of 0.1 mM isopropyl-β-D-thiogalactopyranoside (Sigma). The cells were harvested by centrifugation (4500 rpm, 30 min at 4°C) four hours after induction. Recombinant VIM-26 was purified from the periplasm followed by ion exchange chromatography on a Q-Sepharose HP column (GE Healthcare) and size exclusion chromatography on a Superdex 200 column (GE Healthcare). Buffer A (50 mM Tris pH 7.2, 100 µM $ZnCl_2$) was used for binding during ionic exchange purification, and elution took place during a gradient of Buffer B (Buffer A plus 500 mM NaCl). Size exclusion was carried out in Buffer A. Purified VIM-26 was concentrated by ultrafiltration (3 kDa Cut off, Amicon) to a final concentration of 16.5 mg/ml protein with >95% purity as judged from SDS-PAGE analysis and stored at 4°C. The purified protein was subjected to MS-MS analysis for identification after purification.

Enzyme kinetics on VIM-26

The protein concentration of purified VIM-26 was determined from the absorbance at 280 nm using extinction coefficient 28,420 M^{-1} cm^{-1} calculated from the amino acid sequence at the ProtParam tool at the ExPASy Bioinformatics Resource Portal [www.expasy.org] and a theoretical molecular weight of 25,891 daltons assuming cleavage of the leader sequence at residue Ala20 (Ala16 according to class B β-lactamase (BBL) numbering [35]) as predicted from the SignalP 4.1 Server http://www.cbs.dtu.dk/services/SignalP/

Steady-state enzyme kinetic measurements were completed at 25°C in UV-transparent 96-well plates (Corning) using a SpectraMax 190 spectrophotometer (Molecular Devices) in 50mM HEPES pH 7.2, 100 µM $ZnCl_2$, 0.1 mg/mL bovine serum albumin and 1-10 nM VIM-26. Extinction coefficients for 96-well plates were calculated from standard curves constructed from absorbance measurements of serially diluted unhydrolyzed and completely hydrolyzed substrates. The tested substrates (Figure 1) benzylpenicillin, ampicillin, cefepime, ceftazidime, cefoxitin, cefuroxime, ertapenem, imipenem and meropenem were purchased from Sigma-Aldrich, Panpharma or AppliChem. For each substrate K_M (µM) and k_{cat} (s^{-1}) were determined from plots of initial velocity of hydrolysis against the substrate concentrations. For benzylpenicillin and ampicillin, the K_M was determined as the K_i by measuring inhibition of hydrolysis of the reporter substrate nitrocefin (Calbiochem) across a range of penicillin and nitrocefin concentrations. K_i values were determined by a global (SHARED-parameter) fit of these multiple data sets to a competitive inhibition model. In detail [21], the K_i was determined by the plot of V_o/V_i versus I where V_o and V_i are the initial velocity rates of nitrocefin hydrolysis without (V_o) and with (V_i) inhibitor. In this case the penicillins were the inhibitors. By plotting the V_o/V_i ratio versus the

inhibitor concentration, the slope is $K_M^s/(K_M^s+[S])$ *K_i. Herein, K_M^s is the Michaelis-Menten constant of the substrate nitrocefin, and [S] the concentration of the substrate nitrocefin. All the kinetic data were fitted by nonlinear regression as implemented in the Prism program (GraphPad Software).

Minimum inhibitory concentration (MIC) determination

The *bla* genes encoding VIM-1, VIM-2, VIM-7 or VIM-26 were amplified using Phusion High-Fidelity PCR mastermix (NEB). The following primers were used for amplification: VIM-1 and VIM-26; VIM-1-RBS-F (5'-AGGAGGGTCTTG**ATG**TTAAAAGTTATTAGTAGT) and VIM-1-RBS-R (5'-CTACTACTCGGCGACTGAGCGAT), VIM-2; VIM-2-RBS-F (5'-AGGAGGGTTTTG**ATG**TTCAAACTTTTGAGTAAG) and VIM-2-RBS-R (5'- CTACTCAACGACTGAGCGAT) and VIM-7; VIM-7-RBS-F (5'-AGGAGGGTATTG**ATG**TTTCAAATTCGCAGCTTT) and VIM-7-RBS-R (5'-TTACTCGGCCACCGGGCGTA). For all primers, a ribosomal binding site (RBS) was included (underlined), and the ATG start codon is given in bold. Products were purified as described above before they were blunt cloned into the pCRBluntII-TOPO vector (Invitrogen) according to the manufacturer's descriptions. Clones obtained after transformation of pCRBluntII constructs into competent *Escherichia coli* TOP10 (Invitrogen) cells were selected on LB-plates containing 25 mg/L kanamycin (Sigma) and the correct cloning was confirmed by sequencing. The minimum inhibitory concentration (MIC) of the strains and TOP10 cells were determined for a panel of β-lactams using gradient strips (Liofilchem) according to the manufacturer's instructions.

VIM-26 crystallization, data collection and structure determination

Crystallization trials for recombinant VIM-26 were performed using in-house made screening kits and a Phoenix RE nanolitre crystallization robot (Rigaku), setting up 300 nl protein (16.5 mg/mL) and 300 nl reservoir solution by the sitting drop method in 96-well MRC 2 plates containing 60 µl reservoir. Optimization was done using 24 well pre-greased plates (Hampton Research) by the hanging drop method with 500 µl reservoir solution and drops containing 1 µl reservoir and 1 µl protein. After optimizing, good diffracting crystals were obtained after about 1 week of incubation at room temperature with reservoir solutions containing 21% polyethylene glycol monomethyl ethers (PEG MME) 5K, 0.1 M CHES buffer at pH 9.5, 0.1 M magnesium formate and 4% glycerol. The crystals were cryo protected in 25% PEG MME 5 K, 0.1 M CHES buffer at pH 9.5, 0.1 M magnesium formate and 15% glycerol or 15% ethylene glycol, and then flash frozen in liquid nitrogen. The native VIM-26 and VIM-26-Mono structures were only treated with the cryo, whereas two unsuccessful inhibitor soaks (2-6 min in cryo containing D-captopril) resulted in the VIM-26-W and VIM-26-PEG structures. The X-

ray data were collected at BESSY-II, Berlin, at beamline BL14.1 at 100 K with a wavelength of 0.91841 Å. All data were integrated and scaled with XDS and XSCALE [36].

The phase problem of VIM-26 was solved by the molecular replacement method using the program PHASER [37] and the VIM-7 X-ray structure (PDB ID: 2Y8B)[9] as a search model. From the molecular replacement search in the space group $P2_1$ only one solution with one molecule in the asymmetric unit was found. The models were refined in Phenix [38] and manually built in WinCoot [39].

Docking of ceftazidime into VIM-26 was done using the six reported substrate conformations for hydrolyzed ceftazidime that was thoroughly docked into VIM-7 and VIM-2 [9] and fitting these conformations into the new VIM-26 structures. In brief, the hydrolyzed ceftazidime was fitted into VIM-26, treating the enzyme as a rigid receptor. The aim was to obtain interactions from the carboxylate group on the C8 atom of ceftazidime to the Zn1 ion and from the anionic nitrogen (N5) of β-lactam to Zn2, which is similar to the crystal structure complex of L1 MBL with the hydrolysis product of moxalactam [40].

Author Contributions

Conceived and designed the experiments: HKSL KSWE GEKB ØS. Performed the experiments: KSWE HKSL ØS. Analyzed the data: HKSL KSWE GEKB ØS. Wrote the paper: HKSL GEKB ØS.

Acknowledgments

We are grateful to Trine Josefine Olsen Carlsen for excellent technical assistance. Provision of beamtime at BESSY-II BL14.1 is gratefully acknowledged. This project was supported by the Norwegian Structural Biology Centre (NorStruct), the Research Council of Norway (FRIMEDBIO project number 213808) and Tromsø Research Foundation.

References

1. WHO (2014) World Health Organization: Antimicrobial resistance: globalreport on surveillance, ISBN-978-992-974-156474-156478.
2. Palzkill, T. (2013) Metallo-β-lactamase structure and function, *Annals of the New York Academy of Sciences.* **1277**, 91-104.
3. Patel, G. & Bonomo, R. A. (2013) "Stormy waters ahead": global emergence of carbapenemases, *Front Microbiol.* **4**, 48.
4. Walsh, T. R., Toleman, M. A., Poirel, L. & Nordmann, P. (2005) Metallo-β-lactamases: the quiet before the storm?, *Clin Microbiol Rev.* **18**, 306-325.

5. Rodriguez-Martinez, J. M., Nordmann, P., Fortineau, N. & Poirel, L. (2010) VIM-19, a metallo-β-lactamase with increased carbapenemase activity from *Escherichia coli* and *Klebsiella pneumoniae*, *Antimicrob Agents Chemother.* **54**, 471-476.
6. Samuelsen, Ø., Toleman, M. A., Hasseltvedt, V., Fuursted, K., Leegaard, T. M., Walsh, T. R., Sundsfjord, A. & Giske, C. G. (2011) Molecular characterization of VIM-producing *Klebsiella pneumoniae* from Scandinavia reveals genetic relatedness with international clonal complexes encoding transferable multidrug resistance, *Clin Microbiol Infect.* **17**, 1811-1816.
7. Merino, M., Perez-Llarena, F. J., Kerff, F., Poza, M., Mallo, S., Rumbo-Feal, S., Beceiro, A., Juan, C., Oliver, A. & Bou, G. (2010) Role of changes in the L3 loop of the active site in the evolution of enzymatic activity of VIM-type metallo-β-lactamases, *The Journal of antimicrobial chemotherapy.* **65**, 1950-1954.
8. Zhang, H. & Hao, Q. (2011) Crystal structure of NDM-1 reveals a common β-lactam hydrolysis mechanism, *FASEB J.* **25**, 2574-2582.
9. Borra, P. S., Leiros, H.-K. S., Ahmad, R., Spencer, J., Leiros, I., Walsh, T. R., Sundsfjord, A. & Samuelsen, Ø. (2011) Structural and Computational Investigations of VIM-7: Insights into the Substrate Specificity of VIM Metallo-β-Lactamases, *Journal of molecular biology.* **411**, 174-189.
10. Borra, P. S., Samuelsen, Ø., Spencer, J., Walsh, T. R., Lorentzen, M. S. & Leiros, H.-K. S. (2013) Crystal Structures of *Pseudomonas aeruginosa* GIM-1: Active-Site Plasticity in Metallo-β-Lactamases, *Antimicrob Agents Chemother.* **57**, 848-854.
11. Castanheira, M., Deshpande, L. M., Mendes, R. E., Rodriguez-Noriega, E., Jones, R. N. & Morfin-Otero, R. (2011) Comment on: role of changes in the L3 loop of the active site in the evolution of enzymatic activity of VIM-type metallo-β-lactamases, *The Journal of antimicrobial chemotherapy.* **66**, 684-685; author reply 686.
12. Materon, I. C. & Palzkill, T. (2001) Identification of residues critical for metallo-β-lactamase function by codon randomization and selection, *Protein Science.* **10**, 2556-2565.
13. Samuelsen, Ø., Castanheira, M., Walsh, T. R. & Spencer, J. (2008) Kinetic characterization of VIM-7, a divergent member of the VIM metallo-β-lactamase family, *Antimicrob Agents Chemother.* **52**, 2905-2908.
14. Leiros, H.-K. S., Skagseth, S., Edvardsen, K. S., Lorentzen, M. S., Bjerga, G. E., Leiros, I. & Samuelsen, Ø. (2014) His224 Alters the R2 Drug Binding Site and Phe218 Influences the Catalytic Efficiency of the Metallo-β-Lactamase VIM-7, *Antimicrob Agents Chemother.* **58**, 4826-4836.
15. Yamaguchi, Y., Jin, W., Matsunaga, K., Ikemizu, S., Yamagata, Y., Wachino, J., Shibata, N., Arakawa, Y. & Kurosaki, H. (2007) Crystallographic investigation of the inhibition mode of a VIM-2 metallo-β-lactamase from *Pseudomonas aeruginosa* by a mercaptocarboxylate inhibitor, *J Med Chem.* **50**, 6647-6653.
16. Lassaux, P., Traore, D. A., Loisel, E., Favier, A., Docquier, J. D., Sohier, J. S., Laurent, C., Bebrone, C., Frere, J. M., Ferrer, J. L. & Galleni, M. (2011) Biochemical and structural characterization of the subclass B1 metallo-β-lactamase VIM-4, *Antimicrobial agents and chemotherapy.* **55**, 1248-1255.
17. Johnson, A. P. & Woodford, N. (2013) Global spread of antibiotic resistance: the example of New Delhi metallo-β-lactamase (NDM)-mediated carbapenem resistance, *J Med Microbiol.* **62**, 499-513.
18. Drawz, S. M. & Bonomo, R. A. (2010) Three decades of β-lactamase inhibitors, *Clin Microbiol Rev.* **23**, 160-201.
19. King, A. M., Reid-Yu, S. A., Wang, W., King, D. T., De Pascale, G., Strynadka, N. C., Walsh, T. R., Coombes, B. K. & Wright, G. D. (2014) Aspergillomarasmine A overcomes metallo-β-lactamase antibiotic resistance, *Nature.* **510**, 503-506.
20. Drawz, S. M., Papp-Wallace, K. M. & Bonomo, R. A. (2014) New β-lactamase inhibitors: a therapeutic renaissance in an MDR world, *Antimicrob Agents Chemother.* **58**, 1835-1846.

21. Franceschini, N., Caravelli, B., Docquier, J. D., Galleni, M., Frere, J. M., Amicosante, G. & Rossolini, G. M. (2000) Purification and biochemical characterization of the VIM-1 metallo-β-lactamase, *Antimicrobial agents and chemotherapy.* **44**, 3003-3007.
22. Docquier, J. D., Lamotte-Brasseur, J., Galleni, M., Amicosante, G., Frere, J. M. & Rossolini, G. M. (2003) On functional and structural heterogeneity of VIM-type metallo-β-lactamases, *J Antimicrob Chemother.* **51**, 257-266.
23. Gacar, G. G., Midilli, K., Kolayli, F., Ergen, K., Gundes, S., Hosoglu, S., Karadenizli, A. & Vahaboglu, H. (2005) Genetic and enzymatic properties of metallo-β-lactamase VIM-5 from a clinical isolate of *Enterobacter cloacae*, *Antimicrob Agents Chemother.* **49**, 4400-4403.
24. Murphy, T. A., Catto, L. E., Halford, S. E., Hadfield, A. T., Minor, W., Walsh, T. R. & Spencer, J. (2006) Crystal structure of *Pseudomonas aeruginosa* SPM-1 provides insights into variable zinc affinity of metallo-β-lactamases, *J Mol Biol.* **357**, 890-903.
25. Davies, A. M., Rasia, R. M., Vila, A. J., Sutton, B. J. & Fabiane, S. M. (2005) Effect of pH on the active site of an Arg121Cys mutant of the metallo-β-lactamase from *Bacillus cereus*: implications for the enzyme mechanism, *Biochemistry.* **44**, 4841-4849.
26. Garcia-Saez, I., Docquier, J. D., Rossolini, G. M. & Dideberg, O. (2008) The three-dimensional structure of VIM-2, a Zn-β-lactamase from *Pseudomonas aeruginosa* in its reduced and oxidised form, *J Mol Biol.* **375**, 604-611.
27. Leiros, H.-K. S., Timmins, J., Ravelli, R. B. & McSweeney, S. M. (2006) Is radiation damage dependent on the dose rate used during macromolecular crystallography data collection?, *Acta crystallographica Section D, Biological crystallography.* **62**, 125-132.
28. Ravelli, R. B., Leiros, H.-K. S., Pan, B., Caffrey, M. & McSweeney, S. (2003) Specific radiation damage can be used to solve macromolecular crystal structures, *Structure.* **11**, 217-224.
29. Garau, G., Bebrone, C., Anne, C., Galleni, M., Frere, J. M. & Dideberg, O. (2005) A metallo-β-lactamase enzyme in action: crystal structures of the monozinc carbapenemase CphA and its complex with biapenem, *J Mol Biol.* **345**, 785-795.
30. Yanchak, M. P., Taylor, R. A. & Crowder, M. W. (2000) Mutational analysis of metallo-β-lactamase CcrA from *Bacteroides fragilis*, *Biochemistry.* **39**, 11330-11339.
31. Brown, N. G., Horton, L. B., Huang, W., Vongpunsawad, S. & Palzkill, T. (2011) Analysis of the functional contributions of Asn233 in metallo-β-lactamase IMP-1, *Antimicrobial agents and chemotherapy.* **55**, 5696-5702.
32. Materon, I. C., Beharry, Z., Huang, W., Perez, C. & Palzkill, T. (2004) Analysis of the context dependent sequence requirements of active site residues in the metallo-β-lactamase IMP-1, *J Mol Biol.* **344**, 653-663.
33. Yamaguchi, Y., Takashio, N., Wachino, J., Yamagata, Y., Arakawa, Y., Matsuda, K. & Kurosaki, H. (2010) Structure of metallo-β-lactamase IND-7 from a *Chryseobacterium indologenes* clinical isolate at 1.65-Å resolution, *J Biochem.* **147**, 905-915.
34. Leiros, H.-K. S., Borra, P. S., Brandsdal, B. O., Edvardsen, K. S., Spencer, J., Walsh, T. R. & Samuelsen, Ø. (2012) Crystal Structure of the Mobile Metallo-β-Lactamase AIM-1 from *Pseudomonas aeruginosa*: Insights into Antibiotic Binding and the Role of Gln157, *Antimicrob Agents Chemother.* **56**, 4341-4353.
35. Garau, G., Garcia-Saez, I., Bebrone, C., Anne, C., Mercuri, P., Galleni, M., Frere, J. M. & Dideberg, O. (2004) Update of the standard numbering scheme for class B β-lactamases, *Antimicrob Agents Chemother.* **48**, 2347-2349.
36. Kabsch, W. (1993) Automatic processing of rotation diffraction data from crystals of initially unknown symmetry and cell constants, *J Appl Crystallog.* **24**, 795-800.
37. McCoy, A. J., Grosse-Kunstleve, R. W., Storoni, L. C. & Read, R. J. (2005) Likelihood-enhanced fast translation functions, *Acta Crystallogr D Biol Crystallogr.* **61**, 458-464.
38. Adams, P. D., Afonine, P. V., Bunkoczi, G., Chen, V. B., Davis, I. W., Echols, N., Headd, J. J., Hung, L. W., Kapral, G. J., Grosse-Kunstleve, R. W., McCoy, A. J., Moriarty, N. W., Oeffner, R., Read, R. J., Richardson, D. C., Richardson, J. S., Terwilliger, T. C. & Zwart, P. H. (2010) PHENIX: a

comprehensive Python-based system for macromolecular structure solution, *Acta crystallographica Section D, Biological crystallography.* **D66**, 213-221.
39. Emsley, P., Lohkamp, B., Scott, W. G. & Cowtan, K. (2010) Features and development of Coot, *Acta crystallographica Section D, Biological crystallography.* **66**, 486-501.
40. Spencer, J., Read, J., Sessions, R. B., Howell, S., Blackburn, G. M. & Gamblin, S. J. (2005) Antibiotic recognition by binuclear metallo-β-lactamases revealed by X-ray crystallography, *J Am Chem Soc.* **127**, 14439-14444.

Figure and Tables. Figure legends:

Figure 1

Structural formula of β-lactams. Molecular structures of different penicillins, cephalosporins and carbapenems with their full names and abbreviations used in the text.

Figure 2

The VIM-26 structure. a) Overall ribbon figure of VIM-26 with the L1 (residue 60-66) and L3 (residue 223-240) loops in green. b) The VIM-26 active site with the two zinc ions (green) and zinc coordinating residues (His116, His118, His196, Asp120, Osc221, His263). The adjacent residues Phe61, Tyr67, Trp87, Leu224, Ser228 and Asn233 are also depicted and further described in the text. c) Superimposed VIM-26-Mono (blue, zinc in blue) and the di zinc VIM-26 (orange, zinc in orange).

Figure 3

Actives sites. Final 2Fo-Fc maps for a) VIM-26-Mono (blue at 1.5 σ) and b) VIM-26 (blue at 1.5 σ), c) VIM-26-W (blue at 1.5 σ) and d) VIM-26-PEG (blue at 1.2 σ). In all panels the Fo-Fc Fourier difference maps are show in green (+4.0 σ) and red (-4.0 σ), and residues and waters interacting with the zinc ions are labeled.

Figure 4

Structural comparison. Calculated electrostatic surface potentials of a) VIM-26, b) VIM-2 (PDB ID: 1KO3) and c) VIM-7 (PDB ID: 2Y8B), all with docked ceftazidime into the active sites [9].

Table legends:

Table 1. Steady state kinetic constants for purified VIM-26 for various β-lactams, compared to VIM-1, VIM-2 and VIM-7.

Table 2. MIC values for *E. coli* TOP10 host strain and clones harboring bla_{VIM-26}, bla_{VIM-1}, bla_{VIM-2} or bla_{VIM}

Table 3. X-ray data collection statistics for the VIM-26 structures.

Table 4. Refinement statistics for the VIM-26 structures.

Table 5. Zinc ligand details. a) Inter atomic distances (Å) and b) angles (°) for the Zn-ligands in the active site of the VIM-26-Mono, VIM-26, VIM-26-W and VIM-26-PEG structures.

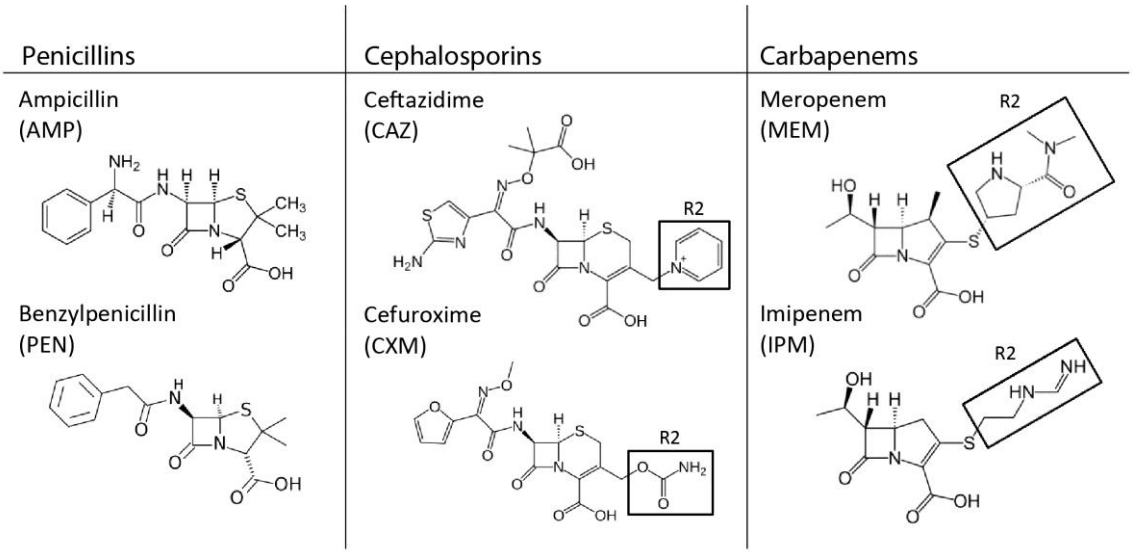

Figure 1 Structural formula of β-lactams.

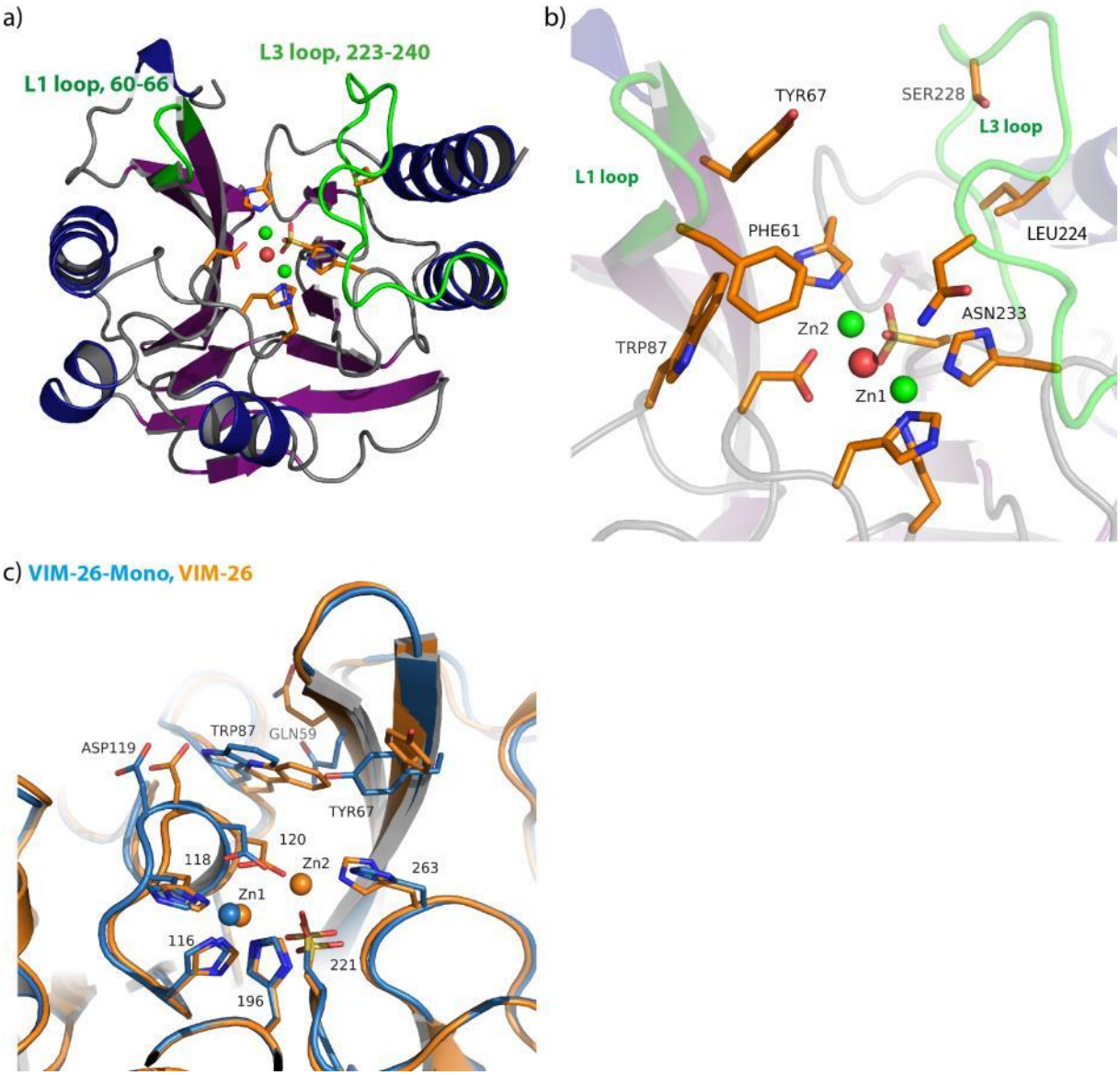

Figure 2 The VIM-26 structure.

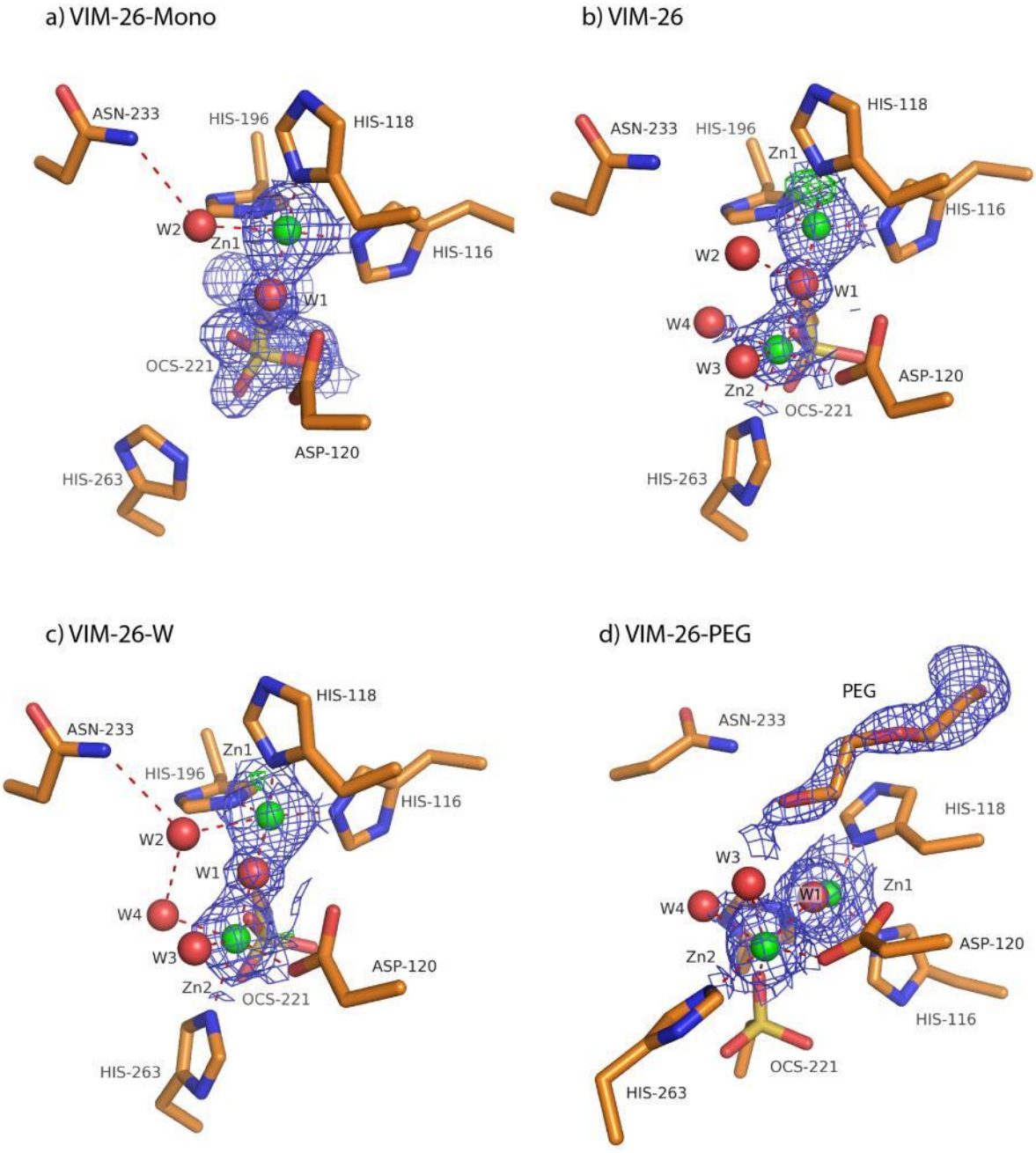

Figure 3 Actives sites

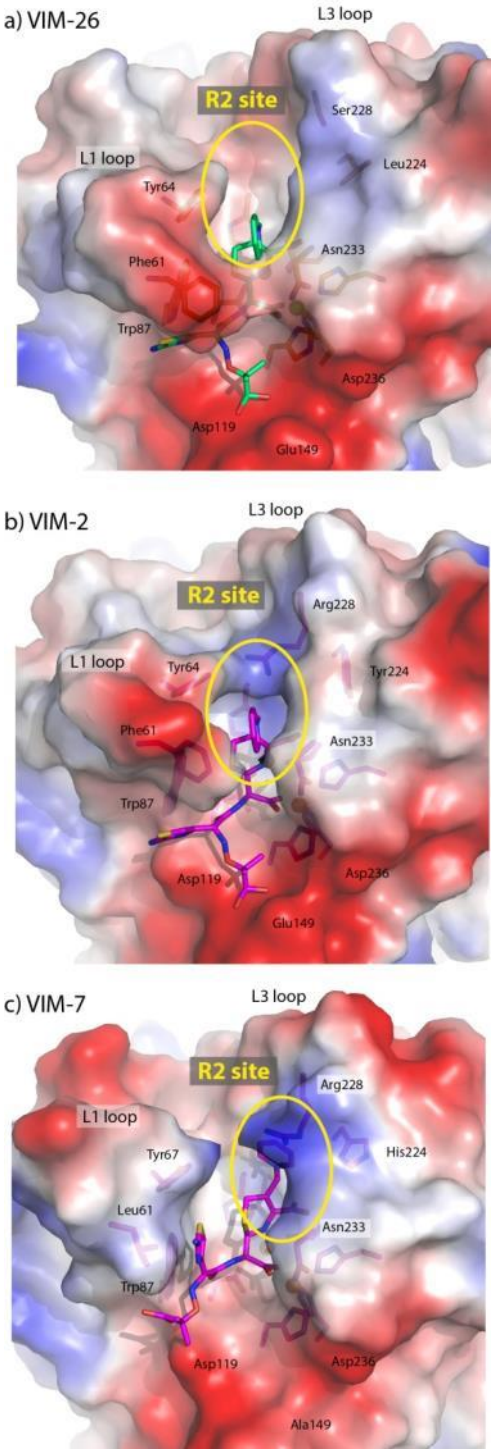

Figure 4 Structural comparison.

Table 1. Steady state kinetic constants for purified VIM-26 for various β-lactams, compared to VIM-1, VIM-2 and VIM-7.

Compound	VIM-26			VIM-1[a]			VIM-2[b]			VIM-7[c]		
	K_M (μM)	k_{cat} (s^{-1})	k_{cat}/K_M ($s^{-1} * \mu M^{-1}$)	K_M (μM)	k_{cat} (s^{-1})	k_{cat}/K_M ($s^{-1} * \mu M^{-1}$)	K_M (μM)	k_{cat} (s^{-1})	k_{cat}/K_M ($s^{-1} * \mu M^{-1}$)	K_M (μM)	k_{cat} (s^{-1})	k_{cat}/K_M ($s^{-1} * \mu M^{-1}$)
Penicillins												
Benzylpenicillin	20 ± 9 [d]	>810	40	841	29	0.034	70	280	4	13.8 [d]	350	25.4
Ampicillin	30 ± 6 [d]	>640	21	917	37	0.04	90	125	1.4	0.56 [d]	38	68
Cephalosporin												
Cefepime	520 ± 70	105 ± 8	0.2	145	549	3.8	>400	>40	0.1	14	0.255	0.018
Ceftazidime	620 ± 90	18 ± 2	0.03	794	60	0.076	72	3.6	0.05	41.8	0.186	0.0044
Cefoxitin	>1120	13 ± 3	0.011	131	26	0.2	13	15	1.2	34	37.51	1.1
Cefuroxime	68 ± 17	140 ± 11	2.05	42	324	7.7	20	8	0.4	9.4	9.9	1.1
Carbapenems												
Ertapenem	280 ± 40	11.4 ± 0.5	0.04	-	-	-	9	0.2	0.022	10.6	3.05	0.29
Imipenem	35 ± 4	11.3 ± 0.4	0.31	1.5	2.0	1.3	9	34	3.8	12.4	47.6	3.84
Meropenem	175 ± 20	37.8 ± 1.4	0.22	48	13	0.27	2	5	2.5	22.4	24.5	1.09

[a] Kinetic constants for VIM-1 taken from [21] which used initial-rate conditions and Hanes-Woolf plots.
[b] Kinetic constants for VIM-2 taken from [22].

[c] Kinetic constants for VIM-7 purified from the periplasm, are taken from [14].

[d] The K_M values were measured as inhibition constants (K_i) in a competitive model using nitrocefin as reporter substrate.

Table 2. MIC values for *E. coli* TOP10 host strain and clones harboring *bla*$_{VIM-26}$, *bla*$_{VIM-1}$, *bla*$_{VIM-2}$ or *bla*$_{VIM-7}$.

	Minimum inhibitory concentration (MIC, mg/L)										
	Penicillins			**Cephalosporins**					**Carbapenems**		
Host strain/clone	AMP	PIP	PTc	CAZ	CTX	CXM	FOX	FEP	MEM	IPM	ETP
TOP10	4	4	8	0,5	0,12	8	4	0,063	0,032	1	0,008
TOP10 pCRBluntII-VIM-26	>256	16	32	64	32	>256	8	2	0,125	4	0,032
TOP10 pCRBluntII-VIM-1	>256	32	128	>256	32	>256	32	8	0,25	2	0,12
TOP10 pCRBluntII-VIM-2	>256	16	32	8	4	128	32	0,25	0,12	0,5	0,06
TOP10 pCRBluntII-VIM-7	32	64	8	0,5	0,25	16	4	0,12	0,06	0,5	0,016

AMP: ampicillin; PIP: piperacillin; PTc: piperacillin-tazobactam; CAZ: ceftazidime; CTX: cefotaxime; CXM: cefuroxime; FOX: cefoxitin; FEP: cefepime: MEM: meropenem; IPM: imipenem; ETP: ertapenem.

Table 3. X-ray data collection statistics for the VIM-26 structures.

X-ray statistics	VIM-26-Mono	VIM-26	VIM-26-W	VIM-26-PEG
PDB Entry	4UWR	4UWO	4UWP	4UWS
Beamline	BL14.1	BL14.1	BL14.1	BL14.1
Space group	$P2_1$	$P2_1$	$P2_1$	$P2_1$
Unit cell (Å)	a=39.74	a=39.63	a=39.69	a=39.76
	b=67.78	b=67.88	b=68.13	b=68.17
	c=40.41	c=40.23	c=40.34	c=40.41
(°)	β=93.07	β =92.39	β =92.60	β=92.56
Resolution (Å)	40-1.55	40-1.55	45-1.70	40.1.66
(highest bin)	(1.63-1.55)	(1.64-1.55)	(1.79-1.70)	(1.75-1.66)
Wavelength (Å)	0.91841	0.91841	0.91841	0.91841
No. of unique reflections	30 941	30 529	22 488	24 661
Multiplicity	4.0 (3.4)	3.4 (3.0)	2.9 (2.2)	3.6 (2.6)
Completeness (%)	99.5 (96.3)	99.6 (97.1)	95.1 (89.7)	96.8 (81.1)
Mean ($\langle I \rangle / \langle \sigma_I \rangle$)	17.3 (3.4)	11.8 (1.9)	11.3 (2.2)	18.6 (2.3)
R_{merge} (%) [a]	4.2 (53.0)	5.7 (61.8)	7.6 (48.4)	4.0 (42.4)
Wilson B-factor (Å^2)	**20.5**	**19.6**	**13.4**	**20.8**

Table 4. Refinement statistics for the VIM-26 structures.

	VIM-26-Mono	VIM-26	VIM-26-W	VIM-26-PEG
Refinement program	Phenix	Phenix	Phenix	Phenix
Resolution (Å)	25.0-1.55	25-1.55	25-1.70	25-1.66
R-factor (all reflections) (%)	15.38	15.26	15.35	15.61
R-free (%)	18.22	18.63	19.40	20.00
No. of non H protein atoms	1938	1913	1910	1959
No. of water molecules	163	163	180	158
Occupancy for Zn1/Zn2	1.0/0.0	1.0/0.50	1.0/0.50	1.0/0.30
R.m.s.d. bond lengths (Å)	0.010	0.010	0.010	0.013
R.m.s.d. bond angles (°)	1.24	1.23	1.26	1.30
Average B-factor (Å^2)				
All atoms	23.20	21.44	23.85	25.34
Protein	20.00	22.18	23.26	24.69
Water molecules	34.60	34.43	35.27	36.09
Zn^{2+} ion(s)	16.02	14.92	15.56	13.92
Ramachandran plot				
Favored (%)	98.0	98.6	98.6	98.3
Allowed (%)	2.0	1.4	1.4	1.7
Outliers (%)	**0**	**0**	**0**	**0**

Table 5. Zinc ligand details. a) Inter atomic distances (Å) and b) angles (°) for the Zn-ligands in the active site of the VIM-26-Mono, VIM-26, VIM-26-W and VIM-26-PEG structures.

a)

		VIM-26-Mono (Å)[#]	VIM-26 (Å)	VIM-26-W (Å)	VIM-26-PEG (Å)
Zn1	His116 NE2	2.09	2.06	2.05	2.06
	His118 ND1	1.98	1.89	1.81	1.89
	His196 NE2	2.02	2.02	2.07	3.00
	W1 (OH^-)	1.90	1.93	1.92	1.97
	W2	2.57	(3.72)	2.95	
Zn2	Asp120 OD2		2.08	2.06	1.95
	Ocs221 OD2		1.98	1.92	1.91
	His263 NE2		2.24	2.36	2.25
	W1 (OH^-)		2.06	2.01	2.25
	W3		2.26	2.41	2.19
	W4		2.11	2.19	2.27
Zn1	**Zn2**		**3.63**	**3.58**	**3.86**

b)

			VIM-26-Mono (°)[1]	VIM-26 (°)	VIM-26-W (°)	VIM-26-PEG (°)
His116 NE2	Zn1	His118 ND1	99.4	98.1	96.3	96.3
	Zn1	His196 NE2	99.8	101.6	97.3	100.1
	Zn1	W1 (OH^-)	100.6	114.0	118.1	111.7
	Zn1	W2	172.7	143.3	165.0	
W1	Zn1	W3		86.5	84.2	88.4
Asp120 OD2	Zn2	Ocs221 OD2		105.3	113.3	118.1
	Zn2	His263NE2		89.4	87.6	100.0
	Zn2	W1 (OH^-)		85.3	90.4	81.7
His263 NE2	**Zn2**	**W1 (OH^-)**		**172.3**	**170.1**	**173.8**

[#] The Zn2 atom is absent in VIM-26-Mono.